Original Research Article

Synthesis, Characterization and Electrochemical Studies on the Corrosion Inhibition Properties of Schiff bases for Mild Steel in 1 M HCl solution.

ABSTRACT

Schiff bases (SBL1 and SBL2), non-toxic compounds were synthesized, characterized and investigated as alternative anticorrosive additives for inhibition of mild steel corrosion in I M HCl acid medium. Corrosion of the steel was monitored by Potentiodynamic Polarization (PDP), Linear Polarization Resistance (LPR), Electrochemical Impedance Spectroscopy (EIS) and Weight Loss (WL) techniques. The novel Schiff base ligands obtained were characterized by Ultraviolet-visible and Fourier-Transform Infrared Spectroscopy. The elemental analysis data for the Schiff base ligands were used to confirm the formula of SBL1 as $C_{17}H_{20}N_2O_2$ and SBL2 as $C_{24}H_{21}N_5O_2$. Fourier-Transform Infrared spectroscopy suggest that the formation of a complex film on the mild steel surface was due to the adsorption of SBL1 and SBL2. The adsorption process was spontaneous and consistent with the mechanism of physical adsorption as best approximated by the Langmuir adsorption isotherm. Maximum inhibition efficiency was obtained at maximum concentration of 100 ppm for both SBL1 and SBL2 with SBL2 possessing the higher inhibition efficiency (86.21%) more than SBL1 (76.92%). Effectiveness of SBL1 and SBL2 reduced with increase in time and progressed with increase in concentration of SBL1 and SBL2. PDP measurements showed that SBL1 and SBL2 acted as a mixed type inhibitor. EIS measurement reveals that the corrosion process was controlled by charge transfer process. Values of the inhibition efficacy obtained from the different techniques were comparable. SEM micrographs of mild steel surface indicated good surface protection of SBL1 and SBL2.

Key word: Schiff bases, Corrosion, Adsorption, inhibitor, Mild steel

1. INTRODUCTION

"The existence of myriad metals have been deeply threatened by corrosion, upon which mild steel constitutes one of them due to its usefulness as structural material for construction works and other industrial equipment which are known to corrode invariably in contact with various solvents (water, moisture and acid solutions)" [1]. "Industrial processes such as acid pickling, industrial cleaning, acid descaling, etching of metal and acidic operations uses acid solutions, especially hydrochloric acid which may cause damage to metal surface via corrosion" [2 – 5].

"Corrosion is the deterioration of the material of construction cum industrial equipment by action of the environment. It is a universal phenomenon occurring in homes, farms, roads, factories, vessels and structures at sea and underground. Corrosion affects the tensile strength and utility efficiency of material thereby degrading the useful properties of the materials and structures including strength, appearance, and permeability to liquids and gases" [6].Corrosion has really affected the gross domestic product (GDP) of many countries which have spent billions of dollar in putting up their industries. Hence, corrosion cost is not only computed in terms of financial losses, but also in terms of human injuries, material replacement, manpower and money.

However, efforts are being made by many industries to combat this menace via electroplating, cathodic protection, anodic protection, alloying elements and the addition of inhibitors.
"A chemical compound which when added to liquid or gas slow down the corrosion rate of a material, typically metal or alloys is known as corrosion inhibitor" [7 – 9]. "Corrosion inhibitors, due to their unique properties are the most convenient means of protecting metals from corrosion process compared to other methods [10]. As a result of the known hazardous effect of most synthetic inhibitors such as chromates, silicates and nitrates coupled with environmental pollution, researchers interest are now directed toward the advancement of eco-friendly less toxic corrosion inhibitors" [3,5].
"Schiff bases possess the above features combined with their structure containing hetero-atoms which make them effective potential corrosion inhibitors for steel, copper and aluminum" [11 – 12]. "Schiff bases are synthesized from primary amines and active carbonyl groups by condensation. The azomethine linkage (HC=N) and the donor atoms in the back bone of the Schiff bases are responsible for their biological and industrial applications, which can be altered depending upon the type of substituent present on the aromatic rings" [9]. "Moreover, the ionic exchange between the mild steel and hetero-atoms such as O, N, P, S and double/triple bonds or aromatic rings plays an important role in the adsorption process" [13 – 14]. "Recently, studies have shown that numerous Schiff base compounds have been reconnoitered as effective acid corrosion inhibitors" [9, 15 – 16]. "The increasing popularity of Schiff bases as corrosion inhibitors is attributed to their low toxicity, high purity, relatively easy synthetic route, low cost of starting materials and environmentally friendly nature" [17]. Generally, the ability of a compound to be adsorbed on the metal surface determine its effectiveness in reducing the rate of corrosion. In view of the above importance of the Schiff bases, we report herein the synthesis and characterization of novel Schiff bases and their attendant effect in inhibiting mild steel corrosion in 1.0 M HCl solution.

2. MATERIAL AND METHOD

2.1 Materials

All reagents used in this study were obtained from Sigma Aldrich, Germany; and were used without further purification. Galenkemp melting point apparatus were used to determine the melting points of the Schiff bases. Elemental analyses (C, H, and N %) were recorded on a Perkin-Elmer model 2400 Series II CNHS/O analyzer. FT-IR spectra of the Schiff base ligands were recorded on a SHIMADZU FTIR-8400 spectrophotometer in the 400-4000cm^{-1} range using KBr matrix. Electronic spectra of the ligands in ethanol solution were scanned in the range 300 - 800 nm on a UV - 2500 PC spectrophotometer. The weight loss measurement were conducted using thermostated water bath, Mettler Toledo PB602 analytical weighing balance and glass wares. Electrochemical studies were performed in a conventional three electrodes cell using computer-controlled potentiostat/galvanostat (Autolab PGSTAT 302N). Different grades of silicon carbide papers in the range of 400 to 1200 were used for surface abrasion.

2.2 Methods

2.2.1 Preparation of Specimens

The mild steel sheet used in this research was obtained from Emma and Sons Nigeria limited, Okigwe, Imo State, Nigeria. The elemental composition of the mild steel by weight percentage was C – 0.17, Si – 0.26, Mn – 0.46, P – 0.0047, S – 0.017 and Fe – 98.935. The mild steel specimens were mechanically pressed cut into coupons of dimension 4 x 3 x 0.017 cm. The coupons were polished with series of emery paper of variable grades starting with the coarsest and then proceeding in steps to the finest grade. They were washed with distilled water, rinsed with absolute ethanol, dried in air after rinsing with acetone which was in accordance with NACE Recommended Practice for surface finishing and cleaning of weight-loss coupons. Also, the coupons were mechanically press cut into coupons of dimensions 10mm by 10mm for electrochemical studies. The specimens were embedded with connecting terminal in epoxy resin leaving a working area of 1 cm^2. The surface preparation of the mechanically abraded specimens was carried out using silicon carbide emery paper of different grades (400 to 1200 grit) and subsequent cleaning with acetone and rinsing with distilled water prior to electrochemical measurement in 1 M HCl solution was prepared by diluting 83ml of 37% HCl (Merck) stock to 1L standard flask with distilled water which was used as corrosive environment. Finely, polished mild steel was exposed to1.0 M HCl in the presence and absence of inhibitors (SBL1and SBL2). The solutions of the Schiff bases having the concentration of 20, 40, 60, 80 and 100 ppm were prepared.

2.2.2 Synthesis of Schiff base Ligand (1) (SBL1)

The Schiff base ligands (SBL1 and SBL2), were synthesized according to literature methods with few modifications [18]. 4-aminophenol (1.36g, 0.01mol) was added to a 30 mL magnetically stirred ethanolic solution of 4-diethylamino-2-hydroxybenzaldehyde (1.74g, 0.01mol) in a 100 mL round bottom flask (Scheme 1). 2.5 mL of glacial acetic acid were added to the mixture to adjust its pH and then refluxed for 6 h upon which a bronze precipitate was formed instantly on cooling. The resulting precipitate was filtered, recrystallized with ethanol and dried in vacuum oven at 80^0C.

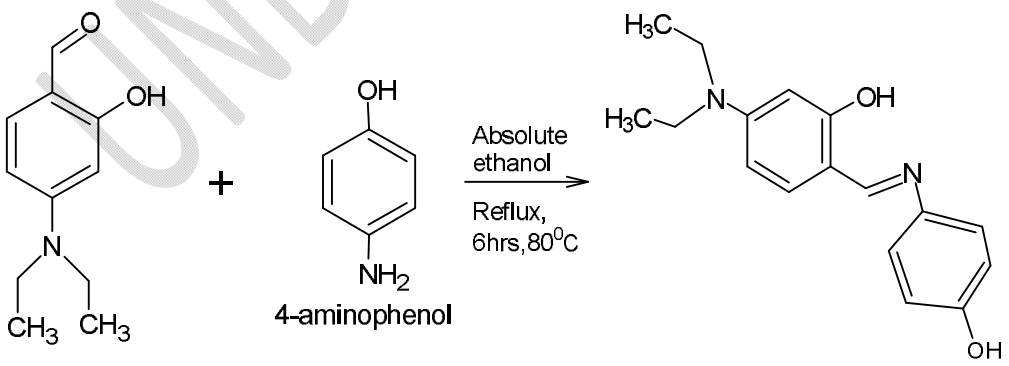

Scheme 1: Synthesis of the Schiff base ligand (1), SBL1, ($C_{17}H_{20}N_2O_2$)

2.2.3 Synthesis of Schiff base Ligand (2) (SBL2)

4-amino antipyrine (2.03g, 0.01mol) was added to a 30 mL magnetically stirred methanolic solution of 4-(Benzeneazo) Salicylaldehyde (2.08 g, 0.01mol) in a 100 mL round bottom flask (Scheme 2). 1.5 ml of glacial acetic acid were added to the mixture, to adjust its pH and then refluxed for 4 h, upon which a teal-green precipitate was formed instantly on cooling. The resulting precipitate was filtered, recrystallized with ethanol and dried in vacuum oven at 80^0C.

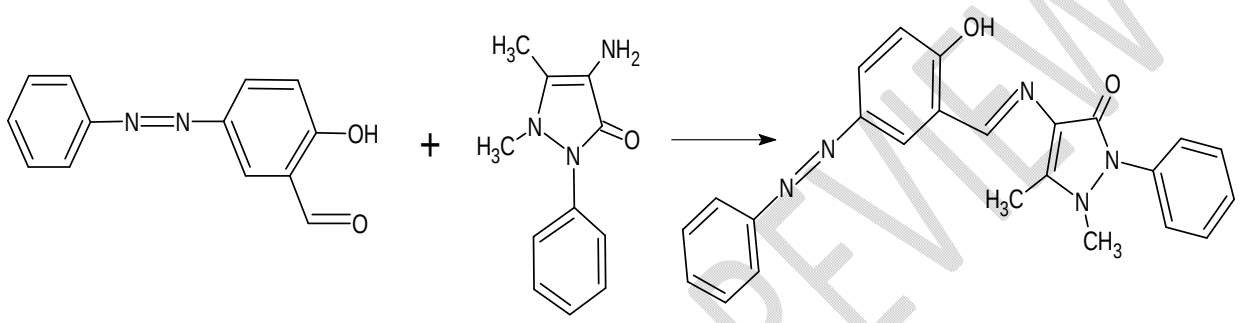

Scheme 2: Synthesis of the Schiff base ligand (2),SBL_2, ($C_{24}H_{21}N_5O_2$)

2.2.4 Solubility Test

The solubility test of the prepared Schiff base ligands were determined in different solvents such as distilled water, ethanol, methanol, dimethylsulfoxide, dimethylformanide, acetone and acetic acid by shaking a small amount of each of the compound in a test tube containing 10 mL portions of each of the solvents.

2.2.5 Melting Point Determination

The melting point of the Schiff bases were determined by introducing a small amount of each samples into a capillary tube and then inserted into Gallenkamp melting point Apparatus, the temperature at which the ligands melted were recorded.

2.2.6 Elemental Analysis

The elemental analysis (CHN) of the Schiff bases were conducted to find the appropriate molecular formula of the compounds and the results obtained using the micro-analytical instrument were compared with the calculated values.

2.2.7 Spectroscopic and Surface Characterization

The electronic absorption spectra also known as UV-Visible are often very useful in structural elucidation. Electronic spectra of the ligands were taken in absolute ethanol (10^{-3}). The IR spectra of the ligands were carried out for structural elucidation and to determine the compounds responsible for adsorption to the metal surface. For weight loss measurements, the coupons were

dipped in 150 mL of 1.0 M of HCl acid containing the studied Schiff base ligands to form an adsorbed layer. The corrosion products were left for three days in 1.0 M HCl without and with 100ppm of the studied inhibitors, after which they were retrieved, dried, and the films scraped. The films were collected and subjected to IR analysis as reported elsewhere [19]. "The samples were prepared using KBr and the analysis were done by scanning the sample through a wave number range of 400–4,000 cm−1" [19 - 20].

2.2.8 Scanning Electron Microscope (SEM) Analysis

Joel JSM-7500F scanning electron microscope (SEM) were used for the morphological studies of the mild steel surfaces exposed to uninhibited and inhibited 1.0 M HCl solutions at room temperature. The recording of the SEM images were achieved in the vacuum mode before and after immersion time of 24 hours in 1.0 M HCl. The instrument was operated at 15 kV.

2.2.9 Gravimetric Technique

"One hundred millilitres (100ml) each of the 1.0M HCl solution was measured into six different beakers with one as the blank (uninhibited solution) and the remaining five labeled A to E containing different concentrations of the inhibitors ranging from 20 ppm to 100 ppm respectively. One mild steel coupon per beaker was used in each experiment. The test coupons were weighed before immersion in the acid solutions and the measurements were taken down. After weighing, the coupons were immersed in the acids solution and then placed in a thermostatic water bath maintained at 303 K. The coupon in each beaker was noted to avoid mix ups during the practical work. The immersion period was two hours intervals, after two hours the coupons were retrieved from the acids, washed with tap water, degreased with ethanol and dried with acetone before the corresponding weights after immersion were recorded. The procedures were repeated for ten hours at 303K. The differences in weight of the coupons were again taken as the weight loss" [21].The corrosion rate (CR), inhibition efficiency (IE), and degree of surface coverage (Ɵ) of mild steel in 1M HCl solution was computed using the formula:

$$\text{Corrosion rate (C.R)} = \frac{\Delta W}{A \times T} \quad (1.1)$$

Where: ΔW = weight loss (g) given as $W_o - W_f$, W_o is the initial weight and W_f the final weight

A = total surface area of the test coupon (cm^2), T = immersion time (hours).

The Inhibition efficiency (IE) defines the level of performance of inhibitor that causes a decrease in corrosion rate. The inhibition efficiency (IE) was computed using the relationship in equation 1.2 (Khaled, 2008).

$$\%IE = \frac{(C.R)o - (C.R)inh}{(C.R)o} \times 100 \quad (1.2)$$

Where: $(C.R)_o$ and $(C.R)_{inh}$ are the corrosion rates in the absence and presence of different concentrations of the inhibitor, respectively.

The surface coverage *(θ)* of the inhibitor was obtained from the experimental data using equation 1.3 as follows:

$$\theta = \frac{(C.R)o - (C.R)inh}{(C.R)o} \quad (1.3)$$

Where: $(C.R)_o$= Corrosion rate in the absence of inhibitor, $(C.R)_{inh}$ = Corrosion rate in the presence of inhibitor.

2.2.10 Electrochemical Measurements

The conventional three electrode set up was used consisting of saturated calomel electrode (SCE) as reference electrode (RE), platinium as counter electrode (CE) and mild steel coupons as working electrode (WE).The area of the working electrode exposed to the medium was approximately 1 cm^2.Fresh solution were used after each sweep. Potentiodynamic polarization measurements were carried out to obtain the information regarding the kinetics of the anodic and cathodic reactions on the mild steel surface. The electrode was allowed to corrode freely before each potentiodynamic polarization (Tafel) study, and its open circuit potential (OCP) was recorded as a function of time up to 1 hour, which was sufficient to attain a stable state. Thereafter, the corrosion potential (E_{corr}) of the working electrode corresponding to a steady-state of OCP was obtained. Potentiodynamic polarization studies were conducted from cathodic to the anodic direction on the potential range ±250 mV versus corrosion potential (E_{corr}) at a scan rate of 10 mV/s.Linear polarization resistance measurements (LPR) were carried out at the potential range ±20 mV with respect to the open circuit potential, and the current response was measured at a scan rate of 0.5 mV/s.This measurement was conducted to support results obtained from PDP measurements. Electrochemical Impendance Spectroscopy **(**EIS) measurements were used to study the characteristic capacitive properties at the mild steel/solution interface, and to affirm the aforementioned electrochemical behavior. The EIS measurements were performed once the OCP was stabilized at a frequency range of 100 KHz to 10 MHz with a signal amplitude perturbation of 5 mV. All electrochemical measurements were carried at room temperature.

The inhibition efficiency (%) from PDP was computed from the measured I_{corr} values using equation (1.4) [22]:

$$I(\%) = \left(\frac{I^o_{corr} - I_{corr}}{I^o_{corr}}\right) \times 100 \quad (1.4)$$

Where I^o_{corr} and I_{corr} are the corrosion current densities in the absence and presence of inhibitor respectively. Stern-Geary equation was used to obtained the polarization resistance (3.9).

$$R_p = \frac{\beta_a \times \beta_c}{2.303 \times l_{corr} \times (\beta_a + \beta_c)} \quad (1.5)$$

Where β_a and β_c are the anodic and cathodic Tafel slopes. From the measured R_p values, the inhibition efficiency (%) was calculated using Equation (1.6).

$$I(\%) = \left(\frac{R_p - R^o_p}{R_p}\right) \times 100 \quad (1.6)$$

Where R^o_p and R_p are the polarization resistance values in the absence and presence of inhibitors.

The constant phase element which is defined by *Yo* and *n* has correlation with the impedance as follows [23]:

$$ZZ_{CPE} = Y_o^{-1}(j\omega)^{-n} \quad (1.7)$$

where Y_o is the CPE constant and n is the CPE exponent, j= $(-1)^{½}$ which is an imaginary number and ω is the angular frequency in rad/s. CPE was used to compensate for the deviation from ideal dielectric behavior arising from the roughness of the mild steel surface. The value of n can be used as a gauge of the heterogeneity or the coarseness of the working electrode surface. The double layer capacitance (C_{dl}) values were calculated from equation (1.8) expression.

$$C_{dl} = \frac{1}{\omega R_{ct}} = \frac{1}{(2\pi f_{max} R_{ct})} \quad (1.8)$$

Where ω is the angular frequency ($\omega = 2\pi f_{max}$), f_{max} is the frequency at which the imaginary component of the impedance is maximum. The inhibition proficiency acquired from the impedance spectroscopy measurements were calculated using equation (1.9):

$$\%IE = \frac{R_{ct(inh)} - R_{ct}^{o}}{R_{ct(inh)}} \times 100 \quad (1.9)$$

Where $R_{ct(inh)}$ and R_{ct}^{o} are the charge transfer resistance in the presence and absence of inhibitor, respectively.

2.2.11 Adsorption Isotherm

"Adsorption isotherm provides information about the adsorbed molecules and their interaction with the metal surface" [24]. "It is the first step in the inhibition process involving Organic inhibitors. Organic inhibitors act by displacing water molecules from the metal surface followed by interaction with anodic and/or cathodic sites. Physisorption and chemisorption adsorption mechanism are the two basic inhibition mechanisms generally considered in discussing the organic inhibitors. Physisorption has to do with the electrostatic interaction between charged metal surface and inhibitor specie. Chemisorption on the other hand involves the sharing of electron pair. The most frequently used isotherms include: Langmuir, Frumkin, Hill de Boer, Parsons, Temkin, Flory-Huggins, Dhar-Flory-Huggins, Bockris-Swinkels and the recently formulated thermodynamic/kinetic model of El-Awady isotherm" [25]. The type of the adsorption isotherm applicable can provide additional information about the properties of the tested compound. All these isotherms are of the general form:

$$f(\theta, x)e^{(-2a\theta)} = KC \quad (2.0)$$

Here $f(\theta, x)$ represents the configuration factor which depends on the physical model and assumptions underlying the derivation of the particular model. K is the adsorption equilibrium constant which describes how strongly the molecules are held on the adsorbent surface and a is the molecular interaction parameter used in the adsorbed layer to predict the nature of interactions. The adsorption isotherms used for the most corrosion inhibition studies are derived from this general form and amended to fit certain purpose(s) and assumptions.

3. Results and Discussion

3.1 Physical Properties of the Schiff Base Ligands

Table1: Physical Properties of the Schiff Base Ligands

Compound	Molecular Formular	Colour	Yield (%)	Melting Point	Elemental Analysis Calculated (Found)		
					C%	H%	N%
SBL1	$C_{17}H_{20}N_2O_2$ (284.37)	Bronze	74.63	187	71.80 (71.20)	7.04 (6.89)	9.85 (9.42)
SBL2	$C_{24}H_{21}N_5O_2$(411)	Teal Green	65.89	192	70.07 (70.62)	5.11 (5.82)	17.03 (17.86)

SBL1= Schiff base ligand (1), SBL2 = Schiff base ligand (2)

The physical properties of the synthesized Schiff bases were analyzed and presented in Table 1. The Schiff base ligands (SBL1 and SBL2) were prepared in good yield, coloured and are air-moisture stable. The colour changes observed were confirmed by the electronic transition from lower to higher energy level. The melting point of SBL1 and SBL2 were found to be 187^{O}C and192^{o}C. This indicated that they are thermally stable ligands. The elemental analysis of the Schiff base ligands (SBL1 and SBL2) were also determined and the percentages of carbon, hydrogen and nitrogen in the compounds were set to be found (Table 1). The values obtained showed a reasonable agreement with the calculated values for the corresponding elements in all the Schiff bases (SBL1 and SBL2). The data for the Schiff bases suggested the formation of $C_{17}H_{20}N_2O_2$ for SBL1 and $C_{24}H_{21}N_5O_2$ for SBL2.

Table 2: Solubility of the Schiff Base Ligands

Compound	Distilled Water	Methanol	Ethanol	Acetic Acid	Acetone	DMSO	DMF
SBL1	IS	SS	SS	S	IS	S	S
SBL2	IS	SS	SS	S	S	S	S

S = Soluble, SS = Slightly Soluble, IS = Insoluble

The solubility of the Schiff base ligands (SBL1 and SBL2) were determined in different solvents. From the result of solubility test presented in Table 2, it can be observed that SBL1 and SBL2 were soluble in acetic acid, dimethylsulfoxide (DMSO) and dimethylformamide (DMF), slightly soluble in ethanol and methanol, and insoluble in water with the exception of SBL2 which was soluble in acetone and SBL1 which was insoluble in acetone.

3.2 Electronic spectra of the Schiff base ligands

Table 3; Electronic Spectroscopic Data for the Schiff base Ligands

Compound	λ_{max}	Assignment
SBL_1	238.5	$n \rightarrow \pi^*$
	306.0	$\pi \rightarrow \pi^*$
SBL_2	249.5	$n \rightarrow \pi^*$
	275.0	$n \rightarrow \pi^*$
	320.5	$\pi \rightarrow \pi^*$

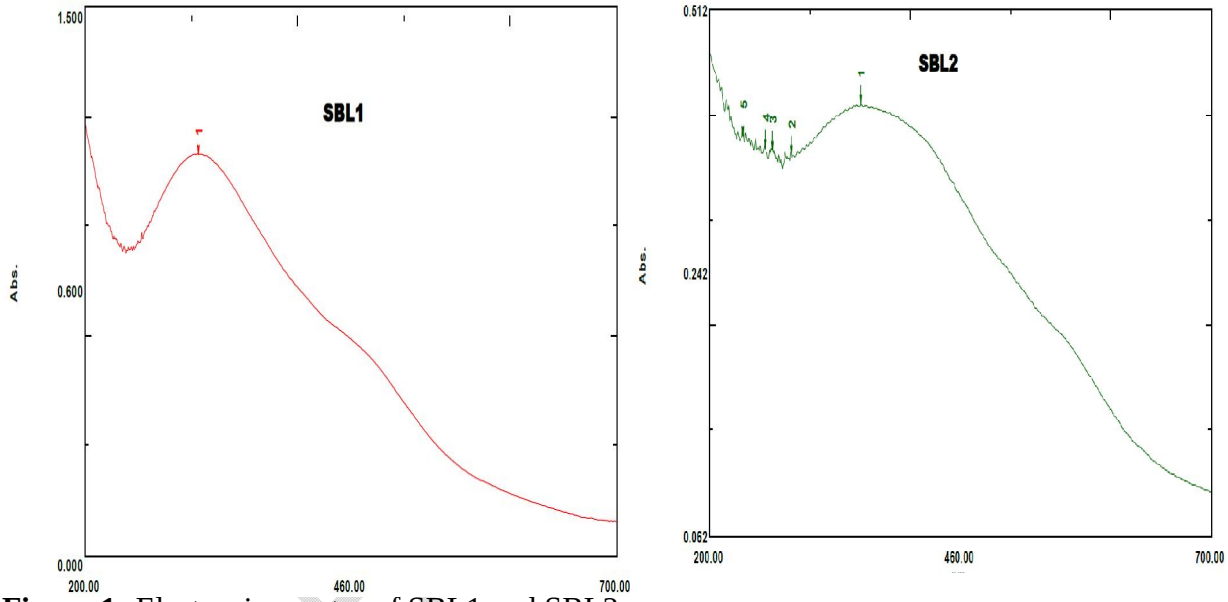

Figure 1: Electronic spectra of SBL1 and SBL2

The electronic spectral data of the Schiff base ligands (SBL1 and SBL2) are given in Table 3. SBL1 showed two major bands at 238.5 nm (41928.72 cm-1) and 306 nm (32679.74 cm-1)while SBL2 showed three essential absorption bands at 249.5nm (40080.16 cm-1), 275.0 nm (36363.64 cm-1) and 320.5 nm (31201.25 cm-1) (Figure 1). The band appearing at lower energy (238.5, 249.5 and 275.0 nm) was attributed to n – π* transition as a result of the non bonding electrons present on the nitrogen atom of the azomethine group (-HC=N) and the phenolic group. The band appearing at higher energy (306 and 320.5 nm) was due to π – π* transition of the ligand centered transitions (LCT) of benzene ring [26 - 27].

3.3 FT-IR spectral analysis

Table 4; The Relevant Infrared Spectra Data for the Schiff base Ligands cm-1

Compound	C-H	C--C	C-O	C-N	C=N	O-H	C-H bend
SBL1	2097.30	1438.80	1326.87	1088.40	1580.40	3250.20	834.90
SBL2	2937.10	1416.40	1326.90	1080.90	1617.70	3369.50	834.90
SBL1 = MS	2922.20	1423.80	1328.90	1088.40	1625.10	3160.80	879.70
SBL2 = MS	2072.40	1490.90	1364.20	1095.80	1595.30	3116.10	827.50

SBL1 = Schiff base ligand 1, SBL2 = Schiff base ligand 2, MS = Mild steel

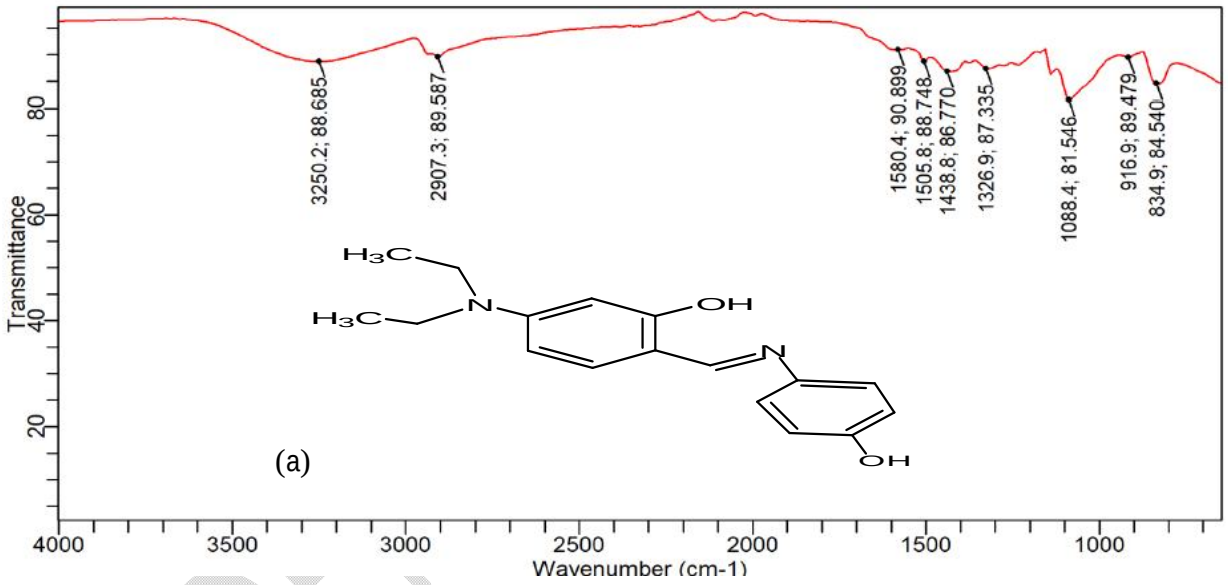

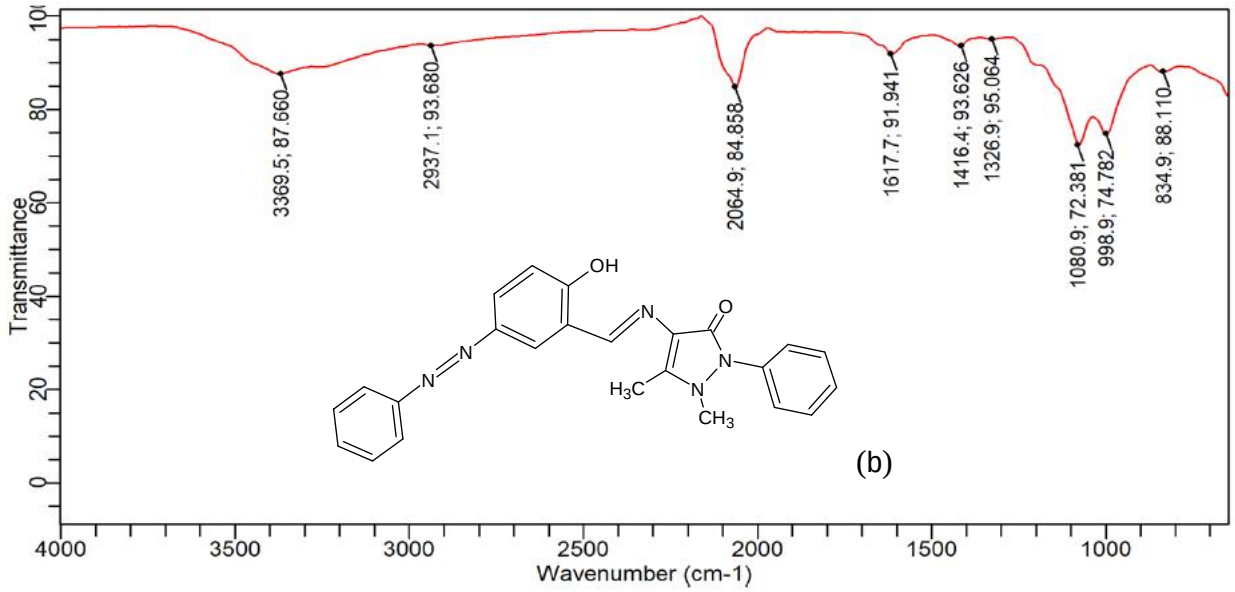

Figure 2: FTIR spectra of (a) SBL1 and (b) SBL2

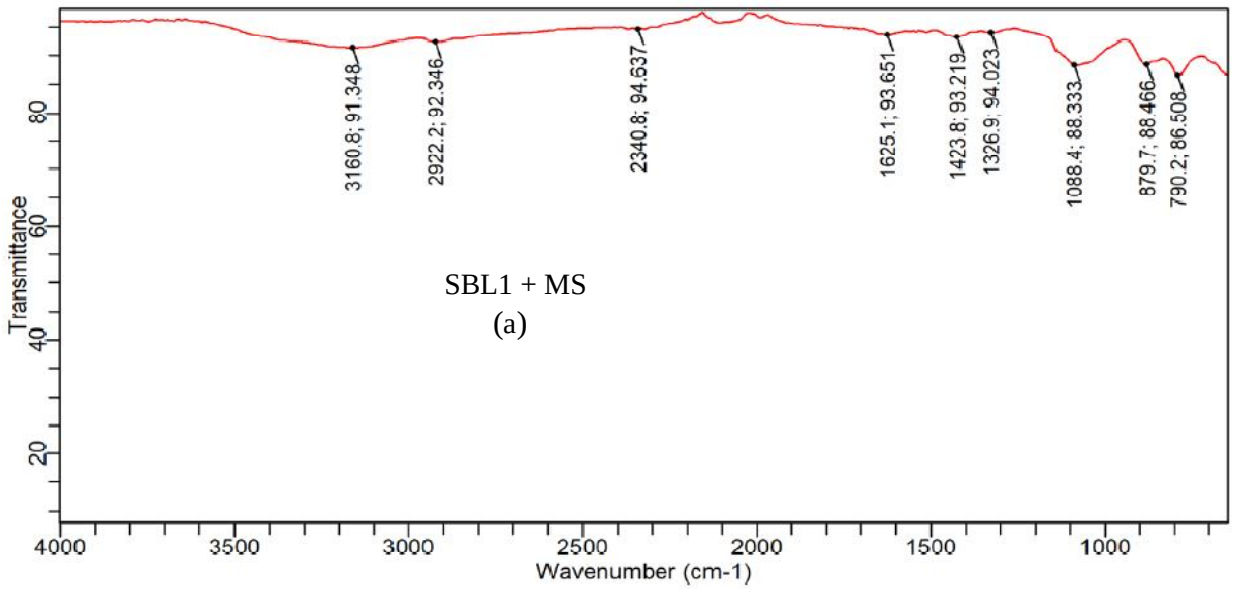

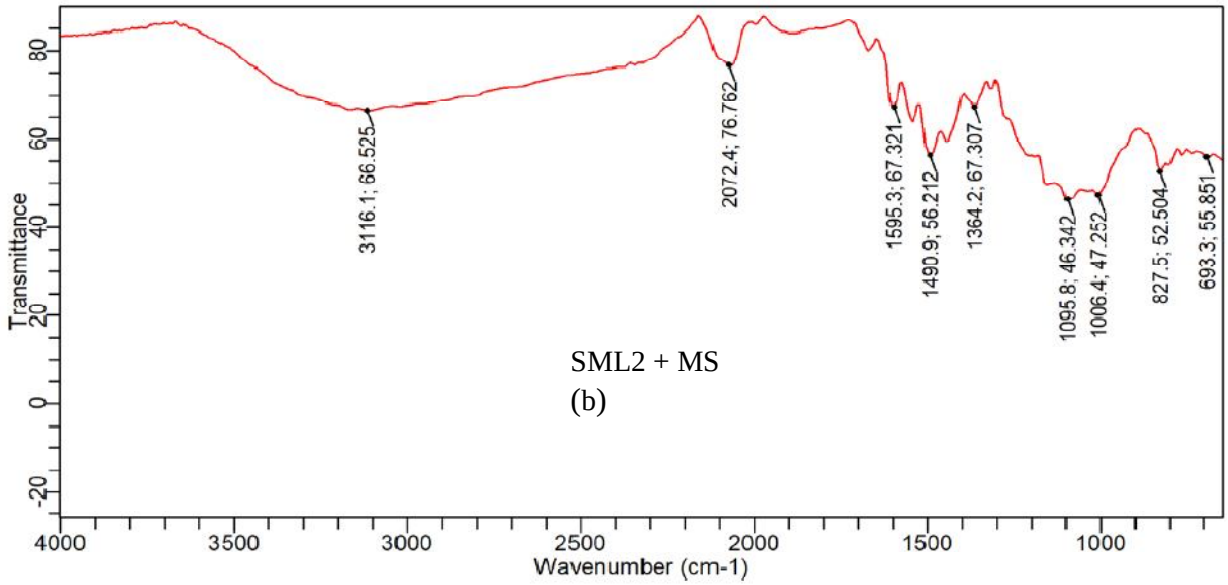

Figure 3: FTIR spectra of the corrosion product of mild steel in 1 M HCl in the presence of (a) SBL1and (b) SBL2

FTIR analysis is used to ascertain the corrosion inhibition process through the adsorption of the Schiff bases (SBL1 and SBL2) on the mild steel surface. The infrared absorption spectra of the Schiff bases and their corrosion products are presented in Table 4. From the results obtained, O-H stretching that obscured the appearance of other peaks give rise to strong and broad peak in the region 3369.50 – 3116.10 cm^{-1}, C-H stretching occurred in the region 2937.10 –2097.30 cm^{-1}, C=N stretching which also obscure the appearance of C=C occurs in the region 1617.70 - 1580.40 cm^{-1}, C-C occurred in the region 1438.80 - 1416.40 cm^{-1}, C-O stretching occurred at 1326.9 cm^{-1},C-N occurred in the region 1088.40 - 1080.90 cm^{-1} and C-H bend occurring at 834.9 $cm^{-1}$for all the Schiff bases. "The IR spectra of the Schiff bases showed peaks attributable to the characteristic functional groups. The presence of these functional groups indicated the effectiveness of the Schiff bases to interact with the mild steel surface and that adsorption between the Schiff bases and the mild steel occurs through the identified functional groups" [3]. Furthermore, by comparing the FT-IR spectrum of the free Schiff base ligands (Figure 2)with the spectra of the corrosion product in the presence of both SBL1 and SBL2 (Figure 3), functional groups responsible for adsorption can be deduced. The spectra of the Schiff bases as well as scraps from the inhibitors films on the surface of the metal are presented in Figures 2 - 3. From the results obtained, the azomethine stretch (C=N) at 1580.4 and 1617.7 cm^{-1} was shifted to 1625.1 and 1595.3 cm^{-1}, C–O stretch at 1326.9 cm^{-1} was shifted to 1328.9 and 1364.2 cm^{-1}, C–C bend at 834.90 cm^{-1} was shifted to 879.7 and 827.5 cm^{-1}, C–C stretch at 1438.8 and 1416.4 $cm^{-1}$was shifted to 1423.8 and 1490.9 cm^{-1}, C-H stretch at 2097.3 and 2937.10 cm^{-1} was shifted to 2922.2 and 2072.4 cm^{-1} , C-N stretch at 1088.4 and 1080.9cm^{-1} was shifted to 1095.8$cm^{-1}$and O–H stretch at 3250.2 and 3369.5 cm^{-1} was shifted to 3160.8 and 3116.1 cm^{-1}. The shifts in frequencies indicated that there was an interaction between the mild steel surface and the Schiff bases. On the other hand, C=C stretch at 1505.80 cm^{-1}, C-H stretch at 2064.90 cm^{-1} and the C-H bend occurred in the region 998.90 - 916.90 cm^{-1} were missing in the spectrum of the corrosion products suggesting that these functional groups were used for the adsorption of the inhibitor

onto the surface of the mild steel [28]. Also, some new bonds were found in the spectrum of the corrosion product. This included the C-H stretch at 2340.80 cm^{-1}, C-N stretch at 1006.4 cm^{-1} and C-H bend at 790.20 and 693 cm^{-1}. This also indicated that some new bonds were also formed through these functional groups [28]. Hence, protection of metallic surface was done via the functional groups presented in the Schiff bases (SBL1 and SBL2).

3.4 Weight Loss Measurements

Table 5. Deduced data for corrosion rate and inhibition efficiency obtained from gravimetric method for mild steel in 1 M HCl after 2 hrs

Compound	Concentration (ppm)	Weight Loss (g)	Corrosion Rate (gcm^{-3} hrs^{-1}) x 10^{-2}	Inhibition Efficiency (%)
SBL1	Blank	0.0130	268.15	--------
	20	0.0071	146.45	45.39
	40	0.0061	125.83	53.08
	60	0.0051	105.20	60.77
	80	0.0039	80.45	70.00
	100	0.0030	61.88	76.92
SBL2	Blank	0.0145	299.09	--------
	20	0.0055	113.45	62.07
	40	0.0040	82.51	72.41
	60	0.0033	68.07	77.24
	80	0.0027	55.69	81.38
	100	0.0020	41.25	86.21

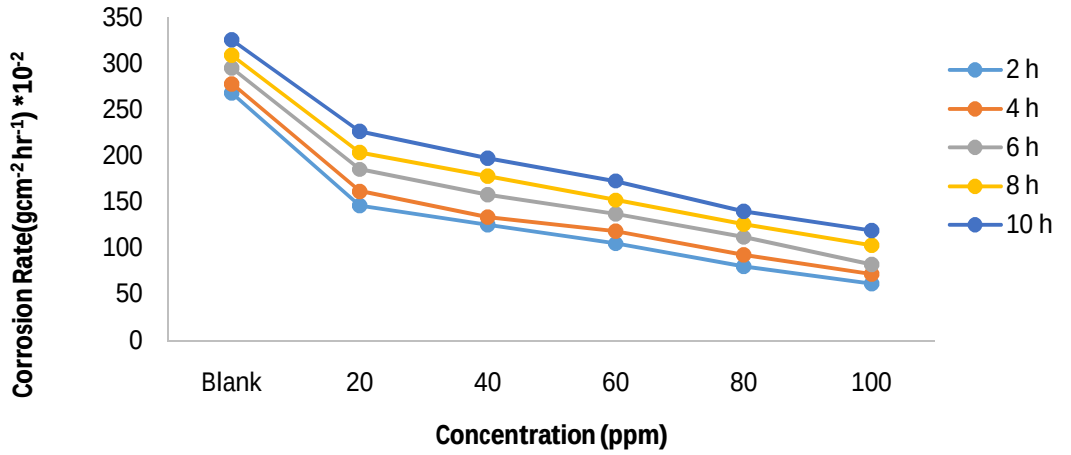

Figure 4 : Variation of corrosion rate with concentration for mild steel coupons in 1 M HCl solution containing SBL1 at different time intervals.

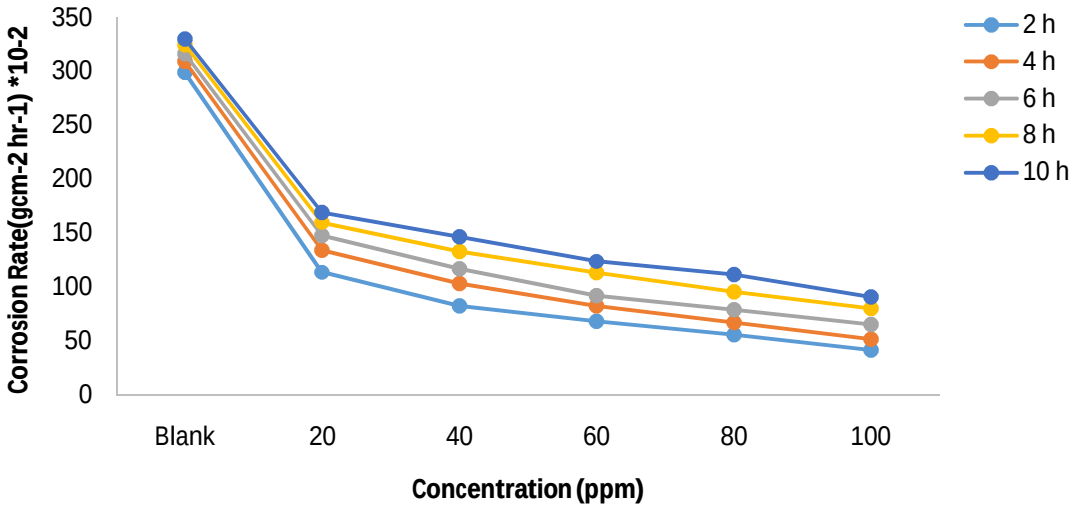

Figure 5 : Variation of corrosion rate with concentration for mild steel coupons in 1 M HCl solution containing the SBL2 at different time intervals.

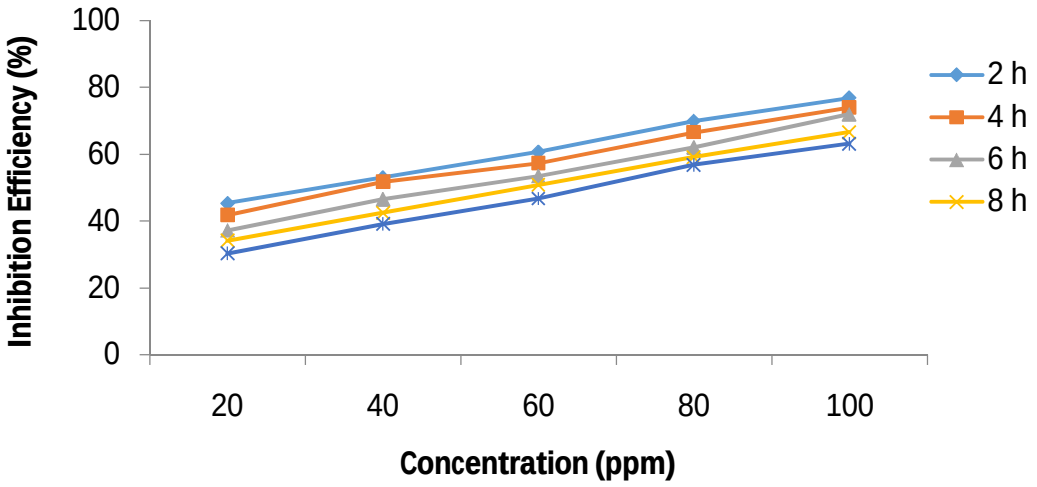

Figure 6 : Variation of inhibition efficiency with concentration of SBL1 at different time intervals.

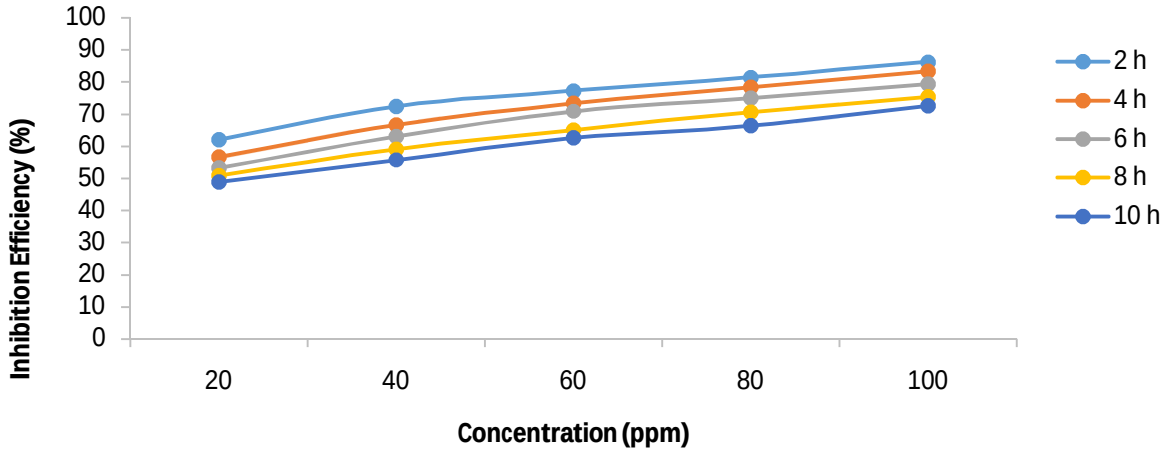

Figure 7: Variation of inhibition efficiency with concentration of SBL2 at different time intervals.

Table 5.indicates that the Schiff bases (SBL1 and SBL2) indeed inhibited the corrosion of mild steel in 1 M hydrochloric acid solution since there was a general decrease in weight loss at the end of the corrosion monitoring process at different time interval. This may be ascribed to the adsorption of inhibitor on the mild steel surface, producing a barrier which isolated the surface from the corrosive environment. It was further supported by increase in corrosion rate in the absence of the inhibitor (blank) but decreased in the presence of the inhibitor and as the concentration of the inhibitor increased at different time intervals (Figures 4 - 5). This decrease is due to the inhibitive effects of the Schiff bases (SBL1 and SBL2). However, there was a

progressive increase in corrosion rate of SBL1 compared to SBL2 and the trend followed SBL1>SBL2.Figures 6 - 7 also showed that the inhibition efficiencies of the Schiff bases in the test solutions increased with increase in concentrations of the inhibitor. Conversely, the inhibition efficiency of SBL2 tends to be higher than SBL1 at the various concentrations under review. Furthermore, the inhibition efficiency of SBL2 was estimated to be 62.07 % even at low concentration (20 ppm) and reached 86.21 % at a concentration of 100 ppm as shown in Table 5. This behaviour was due to the fact that the adsorption coverage of SBL2 inhibitor on metal surface increased with the inhibitor concentration. Such remarkable performances may be due to, the high molecular weight and the presence of abundant electron donation groups (C=N, O-H, C-N, N=N and aromatic rings).

3.5 PDP Measurements

Table 6. PDP parameters for mild steel corrosion in 1 M HCl containing different concentrations of SBL1 and SBL2.

compound	Concentration (ppm)	$-E_{corr}$(mV)	I_{corr} (µA)	β_c(V/dec)	β_a(V/dec)	η%
	Blank (1M HCl)	472	905	65.10	113.70	---------
SBL1	20	480	815	102.30	111.30	9.95
	100	486	689	105.50	124.20	23.87
SBL2	20	494	755	104.00	105.00	16.58
	100	498	630	129.30	137.50	30.39

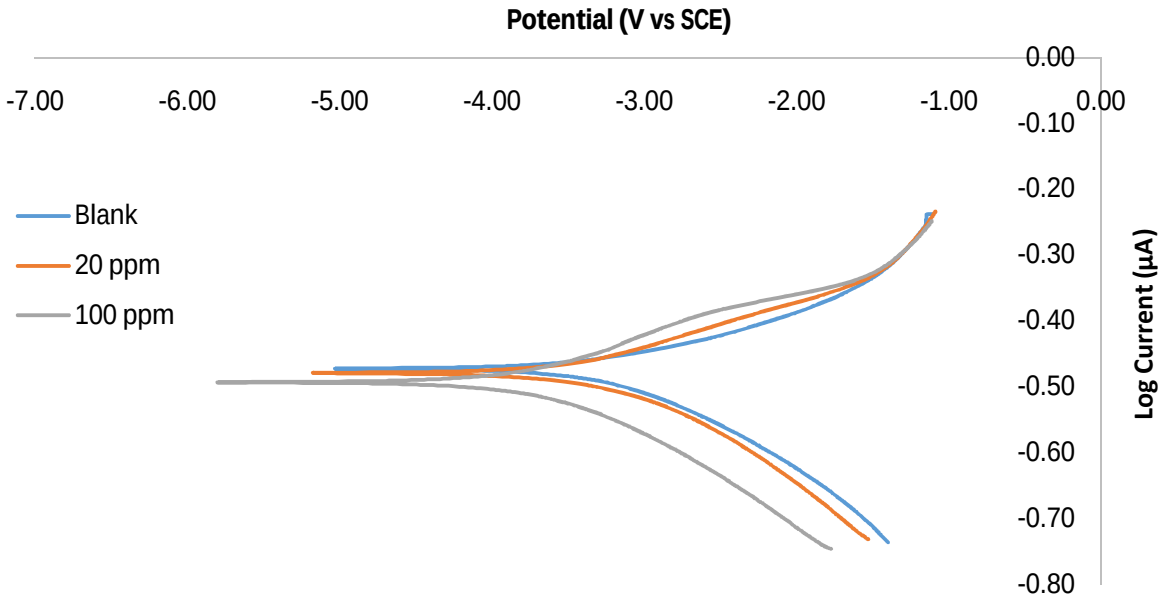

Figure 8. Tafel plots for mild steel corrosion in 1 M HCl containing different concentrations of SBL1.

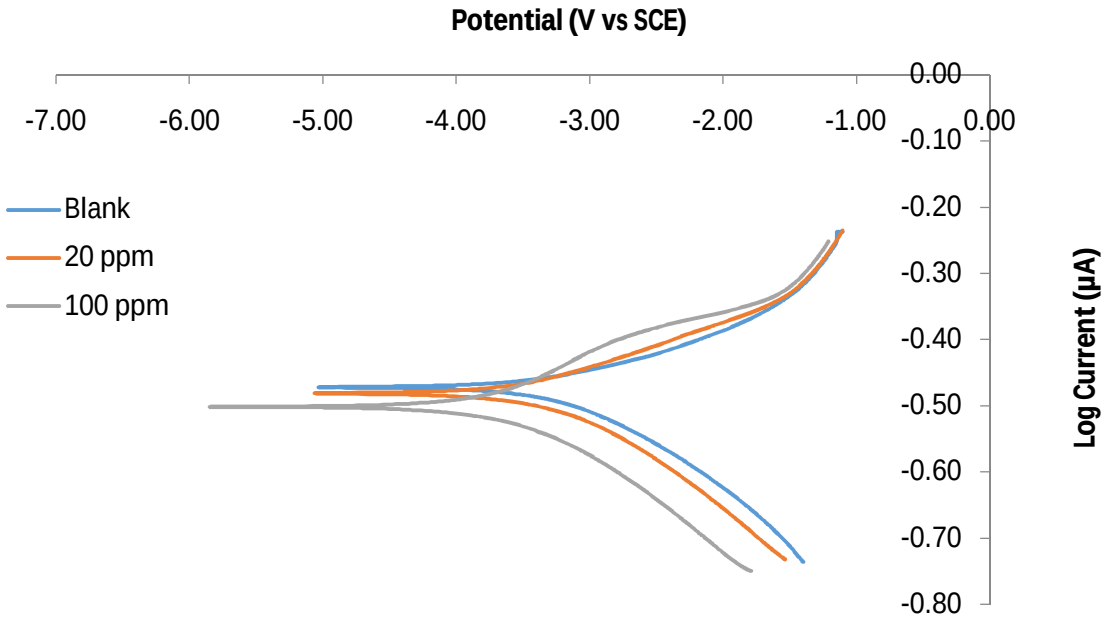

Figure 9. Tafel plots for mild steel corrosion in 1 M HCl containing different concentrations of SBL2.

Potentiodynamic polarization measurements were performed in order to examine the effect of addition of Schiff bases (SBL1 and SBL2) on the corrosion of mild steel in 1 M HCl. Figure 8-9 present the Tafel curves for mild steel in 1 M HCl solution in the absence and presence of the Schiff bases. Mixture of countless metals however constitute the mild steel, with a number of oxidation reactions occurring at the anode. These form of reactions may be represented in Equation (2.0) while the oxidation of iron in the steel sample may be represented by Equation (2.1).

Anode: $M_{(s)} \rightarrow M_{(aq)}^{n+} + ne^{-}$ (2.0)

$Fe_{(s)} \rightarrow Fe_{(aq)}^{2+} + 2e^{-}$ (2.1)

The reduction of water in aqueous environments with sufficiently negative potential (Equation 2.2) and subsequent evolution of hydrogen may also occur at the anode (Equaqtion 2.3).

Cathode: $H_2O + e^{-} \rightarrow H^{+} + OH^{-}$ (2.2)

$2H_{(aq)}^{+} + 2e^{-} \rightarrow H_{2(g)}$ (2.3)

The potential served as the driving force and was controlled to evaluate the current as a function of the net change in reaction rate. The free corrosion current density (I_{corr}) was used to obtain the sum of currents resulting from the electrode processes and the corresponding potential (E_{corr}). The potentiodynamic polarization parameters including corrosion current density (I_{corr}), potential (E_{corr}), cathodic and anodic constants (β_c and β_a) and inhibition efficiency (%) are presented in Table 6. The I_{corr} values declined with an upsurge in inhibitor concentration compared to the free acid solution, forming adsorbed protective layer of the Schiff bases (SBL1 and SBL2) on mild steel surface. Also observed, was that E_{corr} tends to less negative values in the inhibited solutions

compared to the free acid solution (Figure 8 - 9). Anodic inhibitors usually displace E_{corr} to less negative values whereas cathodic inhibitors displace the potential to more negative values [29 - 30]. Consequently, the E_{corr} values obtained suggest that the inhibitors (SBL1 and SBL2) have prevailing influence on the partial anodic and cathodic reaction. However, SBL2 shows greater influence compared to SBL1. Thus, the addition of the Schiff bases further shifted the corrosion potential (E_{corr}) towards negative values but the shift is not up to - 85 mV/SCE to categorize the Schiff base inhibitors as cathodic or anodic type. Such corrosion inhibitors are usually regarded as mixed type inhibitors with anodic predominance [31-32]. The values of β_c and β_a obtained change on addition of inhibitor from that of the free acid solution (Table 6.). The highest difference was obtained with β_a supporting that the Schiff bases (SBL1 and SBL2) exhibits greater influence on anodic reaction than cathodic reaction. The Schiff bases as a mixed type inhibitor functions effectively by forming complex film on some active anodic and cathodic sites of the metal without altering its oxidation mechanism. In other words, Schiff bases (SBL1 and SBL2) actively inhibited both the iron dissolution and hydrogen evolution processes. Similar to EIS results were the calculated values of inhibition efficiency which also increased with an increase in concentration of the inhibitor,.

3.6 LPR measurement

Table 7. LPR parameters for mild steel corrosion in 1 M HCl containing different concentrations of SBL1 and SBL2.

compound	Concentration (ppm)	R_p (Ωcm^2) x 10^{-2}	η%
	Blank (1M HCl)	1.1179	-----
SBL1	20	2.8147	60.28
	100	3.5249	69.16
SBL2	20	3.0037	62.78
	100	4.5939	75.67

Table 7. revealed that values of R_p increased in the presence of the studied inhibitors. The results also showed that R_p values increased with increase in the concentration of the Schiff bases (SBL1 andSBL2).The PDP with respect to concentration followed the same trend as the inhibition efficiency obtained from polarization resistance. Conversely, inhibition efficacy obtained were comparable with EIS results but relatively higher than those from PDP measurements.

3.7 EIS Measurement

Table 8. EIS parameters for mild steel corrosion in 1 M HCl containing different concentrations of SBL1 and SBL2.

EIS Parameters	1 M HCl	20 ppm SBL1	100 ppm SBL1	20 ppm SBL2	100 ppm SBL2
R_{ct} (Ωcm^2)	19.52	115.40	183.10	202.30	356.31
R_s (Ωcm^2)	1.45	1.42	1.39	1.41	1.27
χ^2 x 10^{-4}	8.07	1.06	3.28	0.88	1.31
$Y_{o1}(\Omega s^n cm^{-2})$ x 10^{-4}	3.36	2.43	2.13	2.57	2.00
n_1 x 10^{-1}	8.64	8.33	8.12	8.29	8.08
R_f (Ωcm^2)	5.31	1.04	1.05	0.53	0.85
$Y_{o2}(\Omega s^n cm^{-2})$ x 10^{-2}	6.42	1.95	1.06	5.28	1.94
n_2 x 10^{-1}	1.98	1.86	1.71	0.95	0.61
C_{dl} (µF) x 10^{-2}	8.15	1.38	0.87	0.79	0.66
Ƞ%	------	83.09	89.34	90.11	94.52

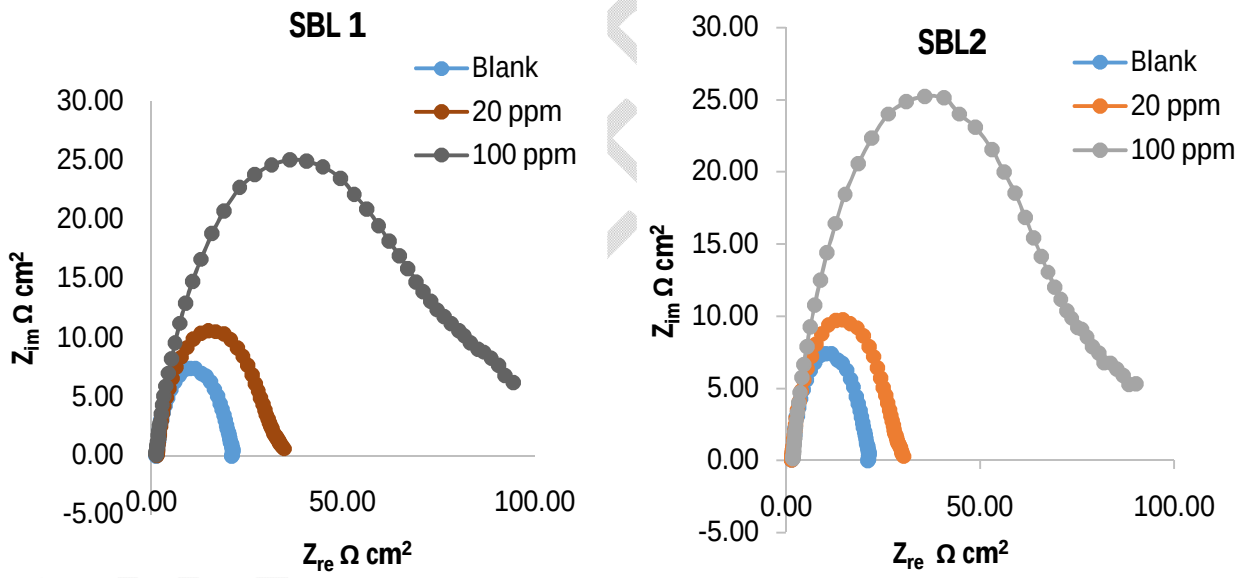

Figure 10.Nyquist plot for inhibition of mild steel corrosion in 1 M HCl in the absence and presence of SBL1 and SBL2.

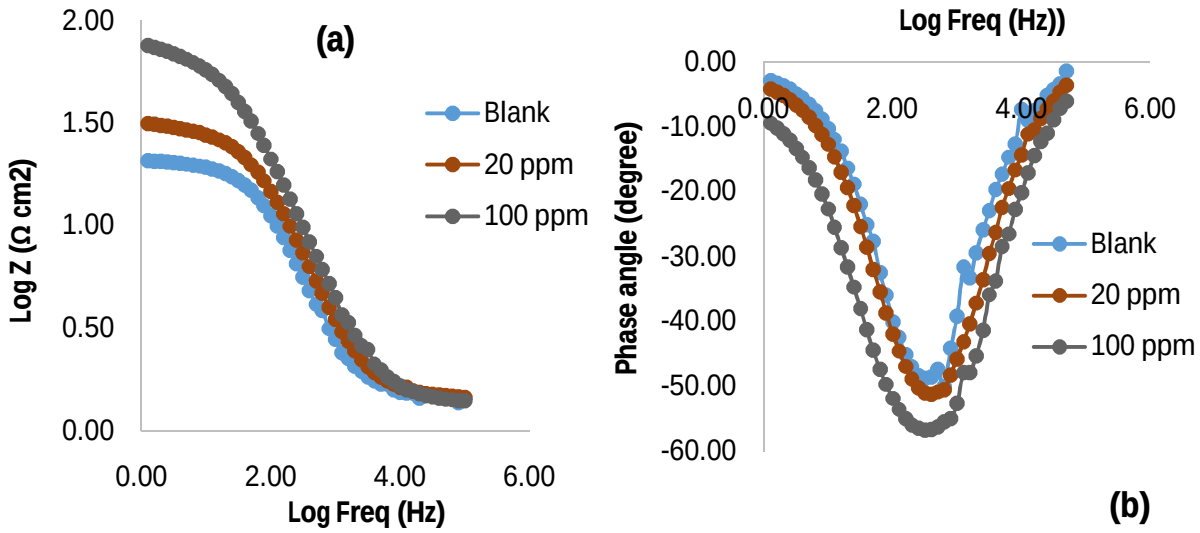

Figure 11. Plots for mild steel in 1 M HCl, in the absence and presence of SBL1 at room temperature in (a) Bode modulus and (b) Bode phase angle representations.

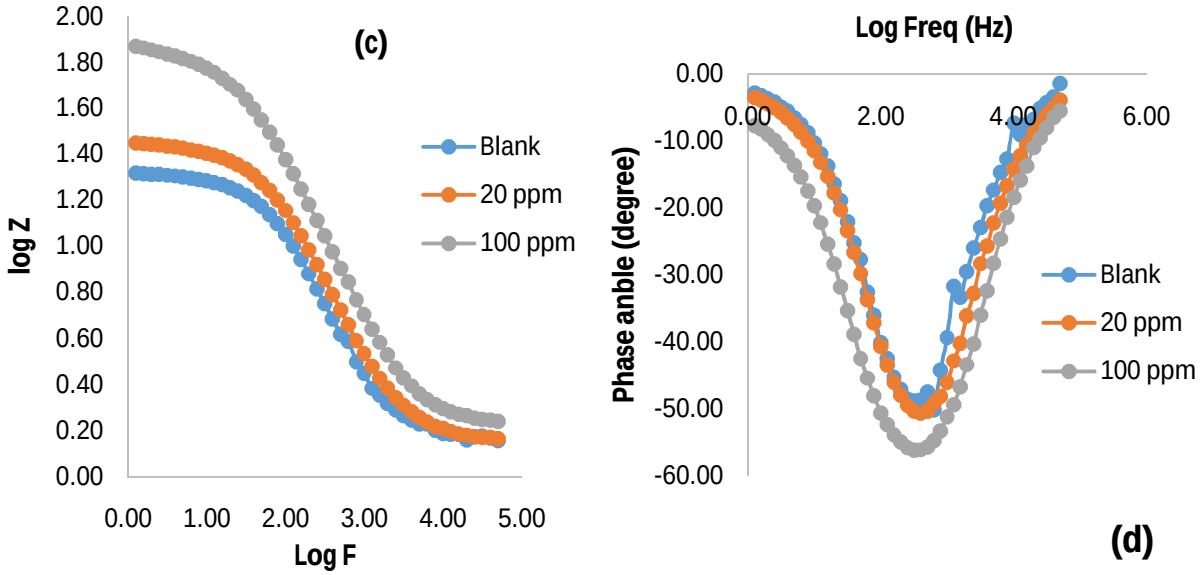

Figure 12. Plots for mild stel in 1 M HCl, in the absence and presence of SBL2 at room temperature in (c) Bode modulus and (d) Bode phase angle representations.

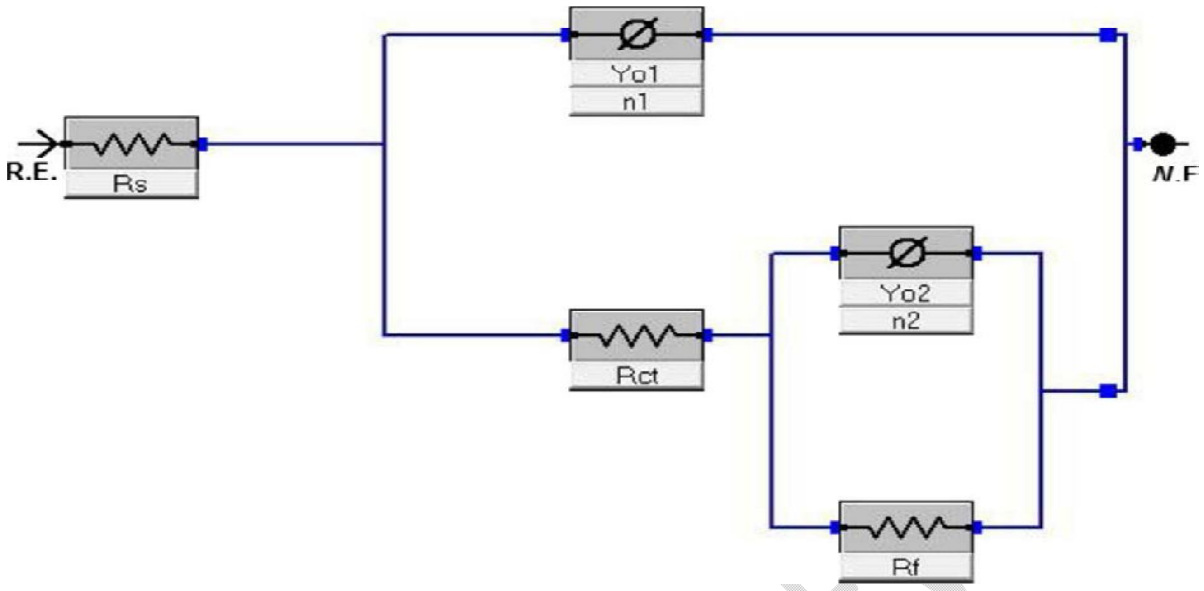

Figure 13. Equivalent circuit used in the analysis of the impedance data.

EIS results for corrosion of mild steel in 1 M HCl in the absence and presence of SBL1 and SBL2 at room temperature were used to obtain Nyquist, Bode modulus and Bode phase angle plots shown in Figure 10 - 12. The presence of the Schiff bases (SBL1 and SBL2) influenced the sizes of their diameters giving rise to an imperfect semicircles (Nyquist plot) as compared to the Blank (1 M HCl). As inhibitor concentration increased the size of the diameters, magnitude of the Bode modulus and the phase angle also increased following the same trend as the calculated inhibition efficiency. However, the addition of SBL2 further increased the diameter of the capacitive loop (Figure 10), magnitude of the Bode modulus (Figure 11a – 12c), and the phase angle (Figure 11b – 12d) compared to SBL1 which was attributed to it large molecular size and presence of more electron donating group giving rise to higher inhibition efficiency in SBL2. Surface roughness of the mild steel is also responsible for the limitation in the shape of the semicircle [29]. "The charge transfer process obtained from the single capacitive loop mainly controlled the mechanism of corrosion" [31]. Adjudged from the analogous shapes of the plots obtained for both inhibited and free acid solution, the mechanism of steel corrosion was not influenced by the introduction of SBL1 and SBL2. The equivalent circuit shown in Figure 13 was used in the analysis of the Nyquist plots. This equivalent circuit was suitable for the modeling of mild steel dissolution in 1 M HCl solution in the absence and presence of the Schiff bases (SBL1 and SBL2) as shown by the values of goodness of fit (χ^2) (Table 8.).The EIS parameters derived from EIS plot (Figure 10 - 12) are presented in Table 8. The value of n which decreased on addition of SBL1 and SBL2, described the extent of roughness or non-homogeneity of the steel surface suggesting that the adsorption of inhibitor molecules on steel surface active sites increased the surface roughness of the steel [30]. An increase in inhibitor concentration increased the charge transfer resistance showing that the 'blanketing' property of the film improved as inhibitor concentration increased. The control effectiveness obtained also developed with increase in inhibitor concentration, hence consistent with weight loss results. The inhibition efficiency increased progressively in the order SBL2 > SBL1.The presence of inhibitors

decreased C_{dl} values. Similar results were obtained by using fluvoxamine-base corrosion inhibitors [30] and 4-(pyridin-4-yl)thiazol-2-amine [33]. "The decrease in C_{dl} values can be attributed to an increase in the thickness of the double layer or decrease in the local dielectric constant caused by the adsorbed protective film of the inhibitors as earlier inferred" [9].

3.8 Adsorption Isotherm

Table 9: Isotherm parameters for the adsorption of SBL1 and SBL2 on the surface of mild steel in HCl at 303 K

Compound	K_{ads}	ΔG_{ads} (KJmol^{-1})	R^2
SBL1	34.483	-19.040	0.974
SBL2	83.333	-21.264	0.997

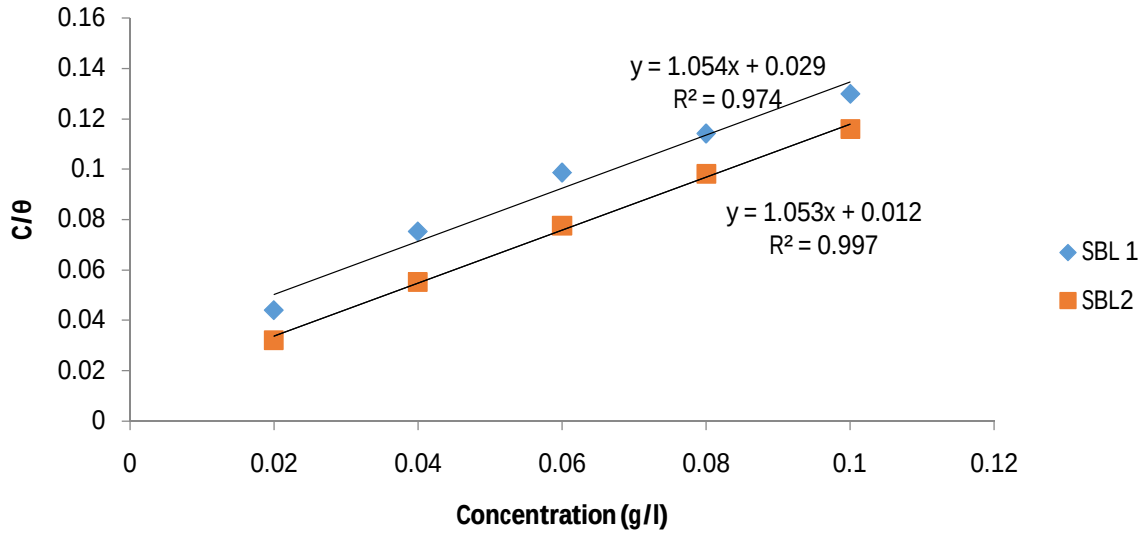

Figure 14: The Langmuir isotherm for the adsorption of SBL1 and SBL2 on mild steel surface in 1.0 M HCl at 303 K

The mode and extent of the interaction between each of the inhibitors (SBL1 and SBL2) and the metal surfaces were studied by applying adsorption isotherms. Surface coverage values (ɳ%/100) from weight loss data were theoretically fitted into different adsorption isotherms and the best fit was adjudged by the value of the linear regression coefficient (R^2) (Table 9). The Langmuir thermodynamic–kinetic adsorption isotherm [34] given by Equation (2.1) gave the best fit.

$$\frac{C}{\theta} = \frac{1}{K_{ads}} + C \qquad (2.1)$$

Where K_{ads} is the equilibrium constant of adsorption, C is the concentration of the inhibitors. K_{ads} is related to the standard free energy of adsorption ($\Delta G°_{ads}$) by the equation as follows:

$$\Delta G°_{ads} = - RTIn(55.5K_{ads}) \qquad (2.2)$$

Where 55.5 is the molar concentration of water molecules expressed in g/L, *R* is the universal gas constant and *T* is the absolute temperature. The inhibitor molecules were spontaneously adsorbed on the metal surface as suggested by the Negative values of ΔG_{ads}, otherwise means nonspontaneous. The mechanism of adsorption was physisorption when the value of $\Delta G_{ads} \leq -20$ kJmol^{-1} and chemisorption when $\Delta G_{ads} \geq -40$ kJmol^{-1} [35]. Straight line graphs were obtained in all cases, indicating that the experimental data fitted well into Langmuir adsorption isotherm model (Figure 14). The adsorption parameters deduced from the linear graph are listed in Table 9. The values of $\Delta G°_{ads}$ were found to be negatively less than the threshold value of −40 kJ mol^{-1}, consistent with the mechanism of physical adsorption revealed that the adsorption of the studied Schiff bases (SBL1 and SBL2) on the mild steel surface was spontaneous [36 -38]. Moreover, the R^2 value of SBL2 tended more closer to unity than SBL1 suggesting SBL2 to be more adsorbed on the metal surface than SBL1 which confirmed the earlier assertion of SBL2 having more electron donor atoms.

3.9 Surface Studies by Scanning Electron Microscopy

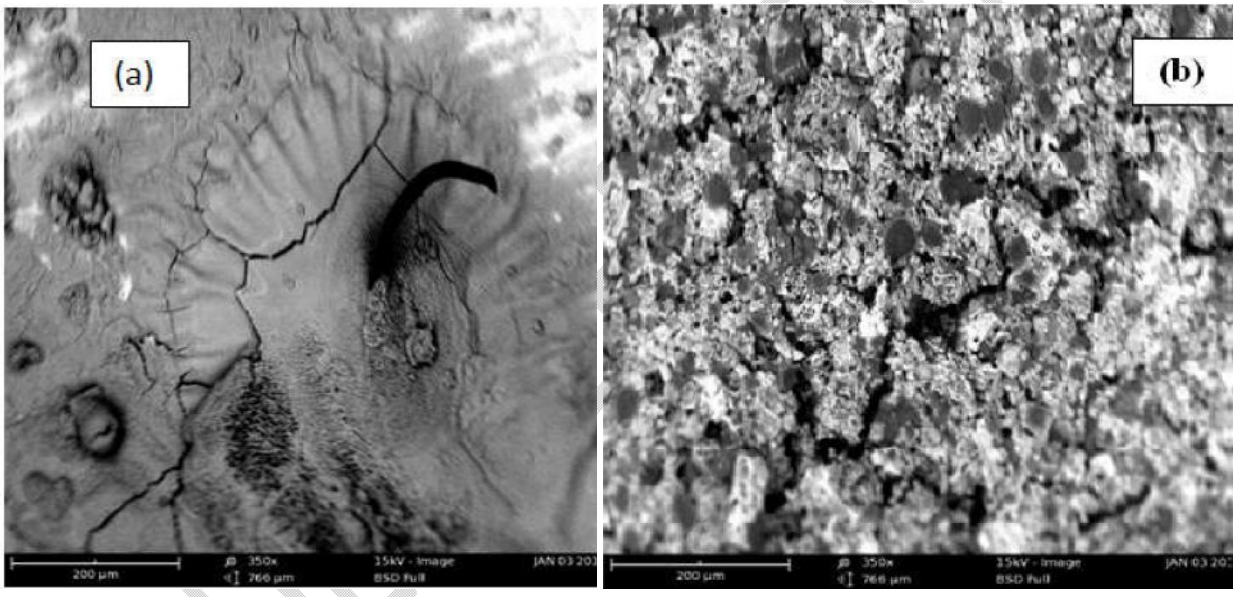

Figure 15. (a) SEM of the mild steel immersed in 1 M HCl solution without inhibitor for 24 h at 200 magnification and (b) SEM of the mild steel immersed in 1 M HCl solution in the presence of the Schiff bases (SBL1 and SBL2)

SEM analysis showed differences in the morphologies of the samples for both the inhibited and uninhibited media. Figure 15. Shows the SEM image of the mild steel surface immersed in the uninhibited medium for 24 h. The observed effect of corrosion on the specimen induced by the acid showed big pits and cracks in the image, leading to the formation and possible evolution of hydrogen gas [39 – 42]. Similar image of mild steel immersed in the inhibited medium is shown in Figure 15. Smoother surfaces with little cracks observed were infused by the complexation due to the formation of a thin film layer between the mild steel and the Schiff bases (SBL1 and SBL2) [42 - 48]. This implies that Schiff bases lowered the corrosion rate which was in agreement with the results obtained from the weight loss analysis.

4. CONCLUSION

The Schiff bases (SBL1 and SBL2) were successfully synthesized and characterized by UV-Visible, FT-IR and CHN-elemental analysis to affirm the proposed structure of the compound. The corrosion inhibition properties of the Schiff bases for mild steel in 1 M HCL solution were investigated. From the results obtained, it can be concluded that all the studied Schiff bases acts as an effective corrosion inhibitor for mild steel in 1M HCl acid solution and their inhibition efficiency increased with increase in the concentration of the Schiff bases with maximum efficiency obtained at an optimum concentration of 100 ppm within the first 2 hours. The electrochemical data were in strong agreement with the chemical data as all the sutdied Schiff bases increased the charged transfer resistance, reduced both the double layer capacitance and corrosion current densities of the interface. Values of E_{corr} also suggested that the Schiff bases acted as mixed type of inhibitors for mild steel. Surface morphology studied by SEM and Fourier transform infrared spectroscopy (FTIR), all indicated that the corrosion reaction was inhibited by the adsorption of the Schiff bases onto the corroding mild steel. The data was best fitted to the Langmuir adsorption isotherm indicating a monolayer chemical adsorption with each inhibitor molecule attached to a single active site of the metal. Hence, Weight loss measurements and Electrochemical measurements (PDP, LPR and EIS) revealed SBL1 and SBL2 as excellent inhibitor for mild steel corrosion in 1M HCl.

REFERENCES

1. Kavitha, V. and Gunavathy, N. Mild Steel Corrosion Inhibition by Daucus carota Pulp Extract in 1 N Hydrochloric Acid Medium. International Journal of Scientific Research in Science and Technology. 2016; 2(6): 249 – 256.
2. Akalezi, C. O., Enenebaku, C. K. and Oguzie, E. E. Application of aqueous extracts of coffee senna for control of mild steel corrosion in acidic environments. International Journal of Industrial Chemistry. 2012; 3: 13–25.
3. Okoronkwo, A.E., Olusegun , S.J. and Olaniran, O. Acid extract of Gliricidia sepium leaves as green corrosion inhibitor for mild steel in HCl solutions. African corrosion Journal. 2015; 1: 30-35.
4. Peter, A. and Sharma, S.K. Use of Azadirachta indica (AZI) as green corrosion inhibitor against mild steel in acidi medium. International Journal of Corrosion Scale Inhibition. 2017; 6(2): 112-131.
5. Akalezi, C.O and Oguzie E.E. Evaluation of anticorrosion properties of chrysophyllum albdum leaves extract for mild steel protection in acidic media. International Journal of Industrial Chemistry. 2016; 7: 81- 92.
6. Samuel .N, Ogah S.P.I, Obike A, Igwe J.C, Ogbonna I.V. Investigation of the Inhibitory Action of Brachystegia Eurycoma (Achi) Seed Extracts on the Corrosion of Mild Steel in 2M HCl by Method of Weight Loss. International Journal Of Scientific Research And Education. 2015; 3: 3744-3753.
7. Leon-Silva, U, Nicho, M, Gonz´alez-Rodr´ıguez, J and Salinas-Bravo, V. Synthesis and characterization of triazol derivative as new corrosion inhibitor for mild steel in 1M HCl solution complemented with antibacterial studies. Journal of Solid State Electrochemistry. 2010; 14: 1089–1100.

8. Gutierrez, E Rodr´ıguez, J. A. Cruz-Borbolla, J. Alvarado-Rodr´ıguez J. G. and Thangarasu, P. Corrosion inhibition of thiadiazole derivative for mild steel in hydrochloric acid solution. Corroion Science Journal. 2016; 108: 23–35.
9. EL Basiony, N. M, Elgendy, A, Nady, H, Migaheda M. A and Zaki E. G. .Adsorption characteristics and inhibition effect of two Schiff base compounds on corrosion of mild steel in 0.5 M HCl solution: experimental, DFT studies, and Monte Carlo simulation. Royal Society of Chemistry Advances. 2019; 9: 10473 – 10485.
10. Haruna, A , Rumah, M.M, Sani, U and Ibrahim, A.K. Synthesis, Characterization and corrosion Inhibition Studies on Mn (II) and Co (II) Complexes Derived from 1-{(Z)-[(2-hydroxyphenyl) imino]methyl}naphthalen-2-ol in 1M HCl Solution.International Journal of Biological, Physical and Chemical Studies. 2020; (3)1: 9-18.
11. Monticelli, C., Balbo, A., Esvan, J., Chiavaric, C., Martini, C., Zanotto, F., Marvelli L and RobbiolaL. Evaluation of 2-(salicylideneimino) thiophenol and other Schiff bases as bronze corrosion inhibitors by electrochemical techniques and surface analysis, Corrosion Science Journal. 2019; (148**):**144–158.
12. Flores-Frias, E.A., Gonzalez-Hernandez, A, Barba, V., Lopez-Sesenes, R, Landeros-Martinez L.L, Flores-De los Rios J.P. and Gonzalez-Rodriguez J.G. Experimental and theoretical evaluation of new 3,3´-methylenedianiline Schiff bases as corrosion inhibitors for carbon steel in sulfuric acid. International Journal of Corrosion Science. 2021; (10)3:1189–1212
13. Jamil D.M., Al‑Okbi A.K, Shaimaa B.A, Ahmed A.A, Abdulhadi K, and Abu, B.M. Experimental and theoretical studies of Schiff bases as corrosion inhibitors. Chemistry Central Journal. 2018; (12):5, 7-16.
14. Ozoemena, C.P, Milam C, and Ugwuoke, M.C. Experimental and theoretical studies on the corrosion inhibitive properties of mild Steel in 2m h2so4 acid solution by ethanolic extract of brachystegia eurycoma seed. Asian Journal of Science and Technology, 2019; 10 (12): 10532-10544.
15. Da Silva, C. M, Da Silva, D. L., Modolo, L. V., Alves, R. B., de Resende, M. A., Martins, C. V. B., and De Fátima, Â. Schiff bases: A short review of their antimicrobial activities. Journal of Advanced Research. 2011; (1)2: 1–8.
16. Zhang, F.,Tang, Y., Cao, Z.,Jing, W., Wu, Z., and Chen, Y. Performance and theoretical study on corrosion inhibition of 2-(4-pyridyl)-benzimidazole for mild steel in hydrochloric acid. Corrosion Science. 2012; 61: 1-9.
17. Saha, S.K, Alokdut, D.C, Pritam G., Dipankar S., and Priyabrata B. Adsorption and corrosion inhibition effect of Schiff base molecules on the mild steel surface in 1 M HCl medium: a combined experimental and theoretical approach. Royal Society of Chemistry. 2015; (17) 4: 5667-5679.
18. Kailas, K. H., Sheetal, J. P., Anita, P. P., and Apoorva, H. P. Four Synthesis Methods of Schiff Base Ligands and Preparation of Their Metal Complex With IR and Antimicrobial Investigation. World Journal of Pharmacy and Pharmaceutical Sciences. 2016; 5(2), 1055–1063.
19. Awe, F.E., Idris, S.O., Abdulwahab, M. and Oguzie, E.E. Theoretical and experimental inhibitive properties of mild steel in HCl by ethanolic extract of Boscia senegalensis. Cogent Chemistry. 2015; 1: 1 - 14.

20. Eddy, N.O. and Odiongenyi, A.O. Corrosion Inhibition and Adsorption Properties of Ethanol Extract of IT heinsia crinata / IT on mild steel in H_2SO_4. Pigment and Resin Technology. 2010; 39 (5): 288-295.
21. Yadav, S., Sharma, A., Choudhary, G., Monika and Sharma A. Inhibitive and adsorption properties of ethanolic extract of fruit of azadirachta indica on the corrosion of copper in HCL. Int. J. Innov. Res. Sci. Eng. Tech. 2014; 3: 16127 – 16136.
22. Roy P., and Sukul D. Corrosion inhibition of mild steel in acidic medium by polyacrylamide grafted Guar gum with various grafting percentage: effect of intramolecular synergism Corrosion Science. 2015; 88**:** 246–253.
23. Arukalam, I.O. Durability and synergistic effects of KI on the acid corrosion inhibition of mild steel by hydroxypropyl methylcellulose, Carbohydrate Polymer. International Journal of Material Science. 2014; 112:291–299.
24. Begum, A.S. Mallika, J. and Gayathri, P. Corrosion Inhibition Property of Some 1, 3, 4- Thiadiazolines on Mild Steel in Acidic Medium. European Journal of Chemistry. 2010; 58: 132 – 144.
25. Abd El-Rehim, S.S., Magdy, A. Ibrahim, M. and Khaled, F. 4-Aminoantipyrine as an inhibitor of mild steel corrosion in HCl solution. Journal of Applied Electrochemistry. 1999; 29(5): 593-599.
26. Boghaei, D. M., Askarizadeh, E., & Bezaatpour, A. Synthesis, characterization, spectroscopic and thermodynamic studies of charge transfer interaction of a new water-soluble cobalt(II) Schiff base complex with imidazole derivatives. Spectrochim Acta A Mol Biomol Spectrosc. 2008; 69(2), 624–628.
27. Shaker, A. M., Nassr, L. A. E and Adam, M. S. S. Hydrophilicity and acid hydrolysis of water-soluble antibacterial iron(II) Schiff base complexes in binary aqueous solvents. Russian Journal of General Chemistry. 2013; 83, 2460–2464.
28. Eddy, N.O., Awe, F.E., Gimba, N.O. and Ebenso, E. E. (2011). Inhibitive effect of Prosopis cineraria on mild steel in acidic media. International Journal of Electrochemical Science, 6: 920 - 931.
29. Anupama, K.K. Corrosion inhibition study of medicinal plant extracts and some of their components for mild steel in acid media. M.Sc Thesis, Department of Chemistry, University of Calicut. 2015; 16.
30. Ituen, E.B, James A.O and O. Akaranta. Fluvoxamine-based corrosion inhibitors for J55 steel in aggressive oil and gas well treatment fluids. Egyptian Journal of Petroleum. 2016; 6: 1 – 12.
31. Solomon, M.M and Umoren, S.A. Electrochemical and gravimetric measurements of inhibition of aluminum corrosion by poly (methacrylic acid) in H_2SO_4 solution and synergistic effect of iodide ions. Journal of Adhesion Science Technology. 2015; 76: 104– 116.
32. Ekerete, J.B, Essien, K. E. and Okafor, P. C. Experimental and quantum studies: a new corrosion inhibitor for mild steel. Elixir International Journal of corrosion and Dye. 2016; 90: 37673 - 37678.
33. Li, F, Yang, X and Zhang, W. 4-(Pyridin-4-yl) thiazol-2-amine as an efficient nontoxic inhibitor for mild steel in hydrochloric acid solutions. Royal Society of Chemistry Advances. 2019; 9: 10454 – 10464

34. Ituen, E.B., Onyewuchi, A. and Abosede, J. (2017). Evaluation of Performance of Corrosion Inhibitors Using Adsorption Isotherm Models: An Overview. Chemical Science International Journal, 18(1): 1-34.
35. Oguzie, E.E. Corrosion inhibition of aluminum in acidic and alkaline media by Sansevieria trifasciata extract. Corrosion Science Journal. 2007; 49: 1527–1539.
36. Ebenso, E. E. Effect of halide ions on the corrosion inhibition of mild steel in H_2SO_4 using methyl red. Bulletin of Electrochemisry. 2004; 19(5): 209 - 216.
37. Khaled, K. F. Corrosion control of copper in nitric acid solutions using some amino acids: A combined experimental and theoretical study. Corrosion Science. 2010; 52: 3225– 3234.
38. Loto, C. A. Inhibition effect of tea (Camellia Sinensis) extract on the corrosion of mild steel in dilute sulphuric acid. Journal of Materials and Environmental Science. 2011; 2: 335 – 344.
39. Fouda, A.S., El-Abbasy, H.M., and El-Sherbini, A.A. Inhibitive effect of *Artemisia judaica* herbs extract on the corrosion of carbon steel in hydrochloric acid solutions. International Journal of Corrosion Scale Inhibition. 2018; 7 (2): 213–235.
40. Obot, I.B., Umoren, S.A., and Ankah, N.K., Pyrazine derivatives as green oil field corrosion inhibitors for steel, J. Mol. Liq., 2019; 277, 749–761.
41. Solomon, M.M., Umoren, S.A., Quraishi, M.A., Tripathi, D.B., and Abai, E.J., Effect of akyl chain length, flow, and temperature on the corrosion inhibition of carbon steel in a simulated acidizing environment by an imidazoline-based inhibitor. 2020; *J. Pet. Sci. Eng.*, 187, 106801.
42. Ugi, B.U., Obeten, M.E., Bassey, M.V., Hitler, L., Adalikwu, S.A., Omaliko, C.E., Nandi, D.O and Uwah, I.E. Adsorption and Inhibition Analysis of Aconitine and Tubocurarine Alkaloids as Eco-friendly Inhibitors of Pitting Corrosion in ASTM – A47 Low Carbon Steel in HCl Acid Environment. Indonesia Journal of Chemistry. 2022; 22 (1): 1 – 16.
43. Tian, Y., and Zheng, M. Inhibition effect of silicate and molybdate on the corrosion of SS 316 in neutral corrosive solution at high temperature, Mater. Res. Express. 2019; 6: 096569.
44. Wang, C., Chen, J., Han, J., Wang, C., and Hu, B. Enhanced corrosion inhibition performance of novel modified polyaspartic acid on carbon steel in HCl solution, J. Alloys Compd., 2019; 771: 736–746.
45. Wang, X., Jiang, H., Zhang, D., Hou, L., and Zhou, W. Solanum lasiocarpum extract as green corrosion inhibitor for A3 steel in 1 M HCl solution, Int. J. Electrochem. Sci., 2019; 14: 1178–1196.
46. Zeino, A., Abdulazeez, I., Khaled, M., Jawich, M.W., and Obot, I.B. Mechanistic study of polyaspartic acid (PASP) as eco-friendly corrosion inhibitor on mild steel in 3% NaCl aerated solution, J. Mol. Liq., 2018; 250: 50–62.
47. Ugi, B.U., Bassey, V.M., Obeten, M.E., Adalikwu, S.A., and Nandi, D.O. Secondary plant metabolites of natural product origin-Strongylodon macrobotrys as pitting corrosion inhibitors of steel around heavy salt deposits in Gabu, Nigeria, J. Mater. Sci. Chem. Eng., 2020; 8 (5): 38–60.

48. Ugi, B. U., Obeten, M. E.. Bassey V. M., BoEkom, E. J., Omaliko, E. C., Ugi F. B., and Uwah I. E. Quantum and Electrochemical Studies of Corrosion Inhibition Impact on Industrial Structural Steel (E410) by Expired Amiloride Drug in 0.5 M Solutions of HCl, H2SO4 and NaHCO3. Moroccan Journal of Chemistry. 2021; 9(4): 677 – 696